Title

Measurements of branching fractions for B+→ρ+γ, B0→ρ0γ, and B0→ωγ

Journal

Physical Review D, 78(11)

ISSN

2470-0010

Authors

Aubert, B
Bona, M
Karyotakis, Y
et al.

Publication Date

2008-12-01

DOI

10.1103/physrevd.78.112001

Measurements of branching fractions for $B^+ \to \rho^+\gamma$, $B^0 \to \rho^0\gamma$, and $B^0 \to \omega\gamma$

B. Aubert,[1] M. Bona,[1] Y. Karyotakis,[1] J. P. Lees,[1] V. Poireau,[1] E. Prencipe,[1] X. Prudent,[1] V. Tisserand,[1] J. Garra Tico,[2] E. Grauges,[2] L. Lopez,[3a,3b] A. Palano,[3a,3b] M. Pappagallo,[3a,3b] G. Eigen,[4] B. Stugu,[4] L. Sun,[4] G. S. Abrams,[5] M. Battaglia,[5] D. N. Brown,[5] R. N. Cahn,[5] R. G. Jacobsen,[5] L. T. Kerth,[5] Yu. G. Kolomensky,[5] G. Lynch,[5] I. L. Osipenkov,[5] M. T. Ronan,[5,*] K. Tackmann,[5] T. Tanabe,[5] C. M. Hawkes,[6] N. Soni,[6] A. T. Watson,[6] H. Koch,[7] T. Schroeder,[7] D. Walker,[8] D. J. Asgeirsson,[9] B. G. Fulsom,[9] C. Hearty,[9] T. S. Mattison,[9] J. A. McKenna,[9] M. Barrett,[10] A. Khan,[10] V. E. Blinov,[11] A. D. Bukin,[11] A. R. Buzykaev,[11] V. P. Druzhinin,[11] V. B. Golubev,[11] A. P. Onuchin,[11] S. I. Serednyakov,[11] Yu. I. Skovpen,[11] E. P. Solodov,[11] K. Yu. Todyshev,[11] M. Bondioli,[12] S. Curry,[12] I. Eschrich,[12] D. Kirkby,[12] A. J. Lankford,[12] P. Lund,[12] M. Mandelkern,[12] E. C. Martin,[12] D. P. Stoker,[12] S. Abachi,[13] C. Buchanan,[13] J. W. Gary,[14] F. Liu,[14] O. Long,[14] B. C. Shen,[14,*] G. M. Vitug,[14] Z. Yasin,[14] L. Zhang,[14] V. Sharma,[15] C. Campagnari,[16] T. M. Hong,[16] D. Kovalskyi,[16] M. A. Mazur,[16] J. D. Richman,[16] T. W. Beck,[17] A. M. Eisner,[17] C. J. Flacco,[17] C. A. Heusch,[17] J. Kroseberg,[17] W. S. Lockman,[17] A. J. Martinez,[17] T. Schalk,[17] B. A. Schumm,[17] A. Seiden,[17] L. Wang,[17] M. G. Wilson,[17] L. O. Winstrom,[17] C. H. Cheng,[18] D. A. Doll,[18] B. Echenard,[18] F. Fang,[18] D. G. Hitlin,[18] I. Narsky,[18] T. Piatenko,[18] F. C. Porter,[18] R. Andreassen,[19] G. Mancinelli,[19] B. T. Meadows,[19] K. Mishra,[19] M. D. Sokoloff,[19] P. C. Bloom,[20] W. T. Ford,[20] A. Gaz,[20] J. F. Hirschauer,[20] M. Nagel,[20] U. Nauenberg,[20] J. G. Smith,[20] K. A. Ulmer,[20] S. R. Wagner,[20] R. Ayad,[21,+] A. Soffer,[21,‡] W. H. Toki,[21] R. J. Wilson,[21] D. D. Altenburg,[22] E. Feltresi,[22] A. Hauke,[22] H. Jasper,[22] M. Karbach,[22] J. Merkel,[22] A. Petzold,[22] B. Spaan,[22] K. Wacker,[22] M. J. Kobel,[23] W. F. Mader,[23] R. Nogowski,[23] K. R. Schubert,[23] R. Schwierz,[23] J. E. Sundermann,[23] A. Volk,[23] D. Bernard,[24] G. R. Bonneaud,[24] E. Latour,[24] Ch. Thiebaux,[24] M. Verderi,[24] P. J. Clark,[25] W. Gradl,[25] S. Playfer,[25] J. E. Watson,[25] M. Andreotti,[26a,26b] D. Bettoni,[26a] C. Bozzi,[26a] R. Calabrese,[26a,26b] A. Cecchi,[26a,26b] G. Cibinetto,[26a,26b] P. Franchini,[26a,26b] E. Luppi,[26a,26b] M. Negrini,[26a,26b] A. Petrella,[26a,26b] L. Piemontese,[26a] V. Santoro,[26a,26b] R. Baldini-Ferroli,[27] A. Calcaterra,[27] R. de Sangro,[27] G. Finocchiaro,[27] S. Pacetti,[27] P. Patteri,[27] I. M. Peruzzi,[27,§] M. Piccolo,[27] M. Rama,[27] A. Zallo,[27] A. Buzzo,[28a] R. Contri,[28a,28b] M. Lo Vetere,[28a,28b] M. M. Macri,[28a] M. R. Monge,[28a,28b] S. Passaggio,[28a] C. Patrignani,[28a,28b] E. Robutti,[28a] A. Santroni,[28a,28b] S. Tosi,[28a,28b] K. S. Chaisanguanthum,[29] M. Morii,[29] J. Marks,[30] S. Schenk,[30] U. Uwer,[30] V. Klose,[31] H. M. Lacker,[31] D. J. Bard,[32] P. D. Dauncey,[32] J. A. Nash,[32] W. Panduro Vazquez,[32] M. Tibbetts,[32] P. K. Behera,[33] X. Chai,[33] M. J. Charles,[33] U. Mallik,[33] J. Cochran,[34] H. B. Crawley,[34] L. Dong,[34] W. T. Meyer,[34] S. Prell,[34] E. I. Rosenberg,[34] A. E. Rubin,[34] Y. Y. Gao,[35] A. V. Gritsan,[35] Z. J. Guo,[35] C. K. Lae,[35] A. G. Denig,[36] M. Fritsch,[36] G. Schott,[36] N. Arnaud,[37] J. Béquilleux,[37] A. D'Orazio,[37] M. Davier,[37] J. Firmino da Costa,[37] G. Grosdidier,[37] A. Höcker,[37] V. Lepeltier,[37] F. Le Diberder,[37] A. M. Lutz,[37] S. Pruvot,[37] P. Roudeau,[37] M. H. Schune,[37] J. Serrano,[37] V. Sordini,[37,‖] A. Stocchi,[37] G. Wormser,[37] D. J. Lange,[38] D. M. Wright,[38] I. Bingham,[39] J. P. Burke,[39] C. A. Chavez,[39] J. R. Fry,[39] E. Gabathuler,[39] R. Gamet,[39] D. E. Hutchcroft,[39] D. J. Payne,[39] C. Touramanis,[39] A. J. Bevan,[40] C. K. Clarke,[40] K. A. George,[40] F. Di Lodovico,[40] R. Sacco,[40] M. Sigamani,[40] G. Cowan,[41] H. U. Flaecher,[41] D. A. Hopkins,[41] S. Paramesvaran,[41] F. Salvatore,[41] A. C. Wren,[41] D. N. Brown,[42] C. L. Davis,[42] K. E. Alwyn,[43] D. Bailey,[43] R. J. Barlow,[43] Y. M. Chia,[43] C. L. Edgar,[43] G. Jackson,[43] G. D. Lafferty,[43] T. J. West,[43] J. I. Yi,[43] J. Anderson,[44] C. Chen,[44] A. Jawahery,[44] D. A. Roberts,[44] G. Simi,[44] J. M. Tuggle,[44] C. Dallapiccola,[45] X. Li,[45] E. Salvati,[45] S. Saremi,[45] R. Cowan,[46] D. Dujmic,[46] P. H. Fisher,[46] K. Koeneke,[46] G. Sciolla,[46] M. Spitznagel,[46] F. Taylor,[46] R. K. Yamamoto,[46] M. Zhao,[46] P. M. Patel,[47] S. H. Robertson,[47] A. Lazzaro,[48a,48b] V. Lombardo,[48a] F. Palombo,[48a,48b] J. M. Bauer,[49] L. Cremaldi,[49] V. Eschenburg,[49] R. Godang,[49,¶] R. Kroeger,[49] D. A. Sanders,[49] D. J. Summers,[49] H. W. Zhao,[49] M. Simard,[50] P. Taras,[50] F. B. Viaud,[50] H. Nicholson,[51] G. De Nardo,[52a,52b] L. Lista,[52a] D. Monorchio,[52a,52b] G. Onorato,[52a,52b] C. Sciacca,[52a,52b] G. Raven,[53] H. L. Snoek,[53] C. P. Jessop,[54] K. J. Knoepfel,[54] J. M. LoSecco,[54] W. F. Wang,[54] G. Benelli,[55] L. A. Corwin,[55] K. Honscheid,[55] H. Kagan,[55] R. Kass,[55] J. P. Morris,[55] A. M. Rahimi,[55] J. J. Regensburger,[55] S. J. Sekula,[55] Q. K. Wong,[55] N. L. Blount,[56] J. Brau,[56] R. Frey,[56] O. Igonkina,[56] J. A. Kolb,[56] M. Lu,[56] R. Rahmat,[56] N. B. Sinev,[56] D. Strom,[56] J. Strube,[56] E. Torrence,[56] G. Castelli,[57a,57b] N. Gagliardi,[57a,57b] M. Margoni,[57a,57b] M. Morandin,[57a] M. Posocco,[57a] M. Rotondo,[57a] F. Simonetto,[57a,57b] R. Stroili,[57a,57b] C. Voci,[57a,57b] P. del Amo Sanchez,[58] E. Ben-Haim,[58] H. Briand,[58] G. Calderini,[58] J. Chauveau,[58] P. David,[58] L. Del Buono,[58] O. Hamon,[58] Ph. Leruste,[58] J. Ocariz,[58] A. Perez,[58] J. Prendki,[58] S. Sitt,[58] L. Gladney,[59] M. Biasini,[60a,60b] R. Covarelli,[60a,60b] E. Manoni,[60a,60b] C. Angelini,[61a,61b] G. Batignani,[61a,61b] S. Bettarini,[61a,61b] M. Carpinelli,[61a,61b,**] A. Cervelli,[61a,61b] F. Forti,[61a,61b] M. A. Giorgi,[61a,61b] A. Lusiani,[61a,61c] G. Marchiori,[61a,61b] M. Morganti,[61a,61b] N. Neri,[61a,61b] E. Paoloni,[61a,61b] G. Rizzo,[61a,61b] J. J. Walsh,[61a] D. Lopes Pegna,[62] C. Lu,[62] J. Olsen,[62] A. J. S. Smith,[62] A. V. Telnov,[62] F. Anulli,[63a] E. Baracchini,[63a,63b] G. Cavoto,[63a] D. del Re,[63a,63b] E. Di Marco,[63a,63b] R. Faccini,[63a,63b] F. Ferrarotto,[63a] F. Ferroni,[63a,63b] M. Gaspero,[63a,63b] P. D. Jackson,[63a] L. Li Gioi,[63a]

M. A. Mazzoni,[63a] S. Morganti,[63a] G. Piredda,[63a] F. Polci,[63a,63b] F. Renga,[63a,63b] C. Voena,[63a] M. Ebert,[64] T. Hartmann,[64] H. Schröder,[64] R. Waldi,[64] T. Adye,[65] B. Franek,[65] E. O. Olaiya,[65] F. F. Wilson,[65] S. Emery,[66] M. Escalier,[66] L. Esteve,[66] S. F. Ganzhur,[66] G. Hamel de Monchenault,[66] W. Kozanecki,[66] G. Vasseur,[66] Ch. Yèche,[66] M. Zito,[66] X. R. Chen,[67] H. Liu,[67] W. Park,[67] M. V. Purohit,[67] R. M. White,[67] J. R. Wilson,[67] M. T. Allen,[68] D. Aston,[68] R. Bartoldus,[68] P. Bechtle,[68] J. F. Benitez,[68] R. Cenci,[68] J. P. Coleman,[68] M. R. Convery,[68] J. C. Dingfelder,[68] J. Dorfan,[68] G. P. Dubois-Felsmann,[68] W. Dunwoodie,[68] R. C. Field,[68] A. M. Gabareen,[68] S. J. Gowdy,[68] M. T. Graham,[68] P. Grenier,[68] C. Hast,[68] W. R. Innes,[68] J. Kaminski,[68] M. H. Kelsey,[68] H. Kim,[68] P. Kim,[68] M. L. Kocian,[68] D. W. G. S. Leith,[68] S. Li,[68] B. Lindquist,[68] S. Luitz,[68] V. Luth,[68] H. L. Lynch,[68] D. B. MacFarlane,[68] H. Marsiske,[68] R. Messner,[68] D. R. Muller,[68] H. Neal,[68] S. Nelson,[68] C. P. O'Grady,[68] I. Ofte,[68] A. Perazzo,[68] M. Perl,[68] B. N. Ratcliff,[68] A. Roodman,[68] A. A. Salnikov,[68] R. H. Schindler,[68] J. Schwiening,[68] A. Snyder,[68] D. Su,[68] M. K. Sullivan,[68] K. Suzuki,[68] S. K. Swain,[68] J. M. Thompson,[68] J. Va'vra,[68] A. P. Wagner,[68] M. Weaver,[68] C. A. West,[68] W. J. Wisniewski,[68] M. Wittgen,[68] D. H. Wright,[68] H. W. Wulsin,[68] A. K. Yarritu,[68] K. Yi,[68] C. C. Young,[68] V. Ziegler,[68] P. R. Burchat,[69] A. J. Edwards,[69] S. A. Majewski,[69] T. S. Miyashita,[69] B. A. Petersen,[69] L. Wilden,[69] S. Ahmed,[70] M. S. Alam,[70] J. A. Ernst,[70] B. Pan,[70] M. A. Saeed,[70] S. B. Zain,[70] S. M. Spanier,[71] B. J. Wogsland,[71] R. Eckmann,[72] J. L. Ritchie,[72] A. M. Ruland,[72] C. J. Schilling,[72] R. F. Schwitters,[72] B. W. Drummond,[73] J. M. Izen,[73] X. C. Lou,[73] F. Bianchi,[74a,74b] D. Gamba,[74a,74b] M. Pelliccioni,[74a,74b] M. Bomben,[75a,75b] L. Bosisio,[75a,75b] C. Cartaro,[75a,75b] G. Della Ricca,[75a,75b] L. Lanceri,[75a,75b] L. Vitale,[75a,75b] V. Azzolini,[76] N. Lopez-March,[76] F. Martinez-Vidal,[76] D. A. Milanes,[76] A. Oyanguren,[76] J. Albert,[77] Sw. Banerjee,[77] B. Bhuyan,[77] H. H. F. Choi,[77] K. Hamano,[77] R. Kowalewski,[77] M. J. Lewczuk,[77] I. M. Nugent,[77] J. M. Roney,[77] R. J. Sobie,[77] T. J. Gershon,[78] P. F. Harrison,[78] J. Ilic,[78] T. E. Latham,[78] G. B. Mohanty,[78] H. R. Band,[79] X. Chen,[79] S. Dasu,[79] K. T. Flood,[79] Y. Pan,[79] M. Pierini,[79] R. Prepost,[79] C. O. Vuosalo,[79] and S. L. Wu[79]

(*BABAR* Collaboration)

[1]*Laboratoire de Physique des Particules, IN2P3/CNRS et Université de Savoie, F-74941 Annecy-Le-Vieux, France*
[2]*Universitat de Barcelona, Facultat de Fisica, Departament ECM, E-08028 Barcelona, Spain*
[3a]*INFN Sezione di Bari, I-70126 Bari, Italy*
[3b]*Dipartmento di Fisica, Università di Bari, I-70126 Bari, Italy*
[4]*University of Bergen, Institute of Physics, N-5007 Bergen, Norway*
[5]*Lawrence Berkeley National Laboratory and University of California, Berkeley, California 94720, USA*
[6]*University of Birmingham, Birmingham, B15 2TT, United Kingdom*
[7]*Ruhr Universität Bochum, Institut für Experimentalphysik 1, D-44780 Bochum, Germany*
[8]*University of Bristol, Bristol BS8 1TL, United Kingdom*
[9]*University of British Columbia, Vancouver, British Columbia, Canada V6T 1Z1*
[10]*Brunel University, Uxbridge, Middlesex UB8 3PH, United Kingdom*
[11]*Budker Institute of Nuclear Physics, Novosibirsk 630090, Russia*
[12]*University of California at Irvine, Irvine, California 92697, USA*
[13]*University of California at Los Angeles, Los Angeles, California 90024, USA*
[14]*University of California at Riverside, Riverside, California 92521, USA*
[15]*University of California at San Diego, La Jolla, California 92093, USA*
[16]*University of California at Santa Barbara, Santa Barbara, California 93106, USA*
[17]*University of California at Santa Cruz, Institute for Particle Physics, Santa Cruz, California 95064, USA*
[18]*California Institute of Technology, Pasadena, California 91125, USA*
[19]*University of Cincinnati, Cincinnati, Ohio 45221, USA*
[20]*University of Colorado, Boulder, Colorado 80309, USA*
[21]*Colorado State University, Fort Collins, Colorado 80523, USA*
[22]*Technische Universität Dortmund, Fakultät Physik, D-44221 Dortmund, Germany*
[23]*Technische Universität Dresden, Institut für Kern- und Teilchenphysik, D-01062 Dresden, Germany*
[24]*Laboratoire Leprince-Ringuet, CNRS/IN2P3, Ecole Polytechnique, F-91128 Palaiseau, France*
[25]*University of Edinburgh, Edinburgh EH9 3JZ, United Kingdom*
[26a]*INFN Sezione di Ferrara, I-44100 Ferrara, Italy*
[26b]*Dipartimento di Fisica, Università di Ferrara, I-44100 Ferrara, Italy*
[27]*INFN Laboratori Nazionali di Frascati, I-00044 Frascati, Italy*
[28a]*INFN Sezione di Genova, I-16146 Genova, Italy*
[28b]*Dipartimento di Fisica, Università di Genova, I-16146 Genova, Italy*
[29]*Harvard University, Cambridge, Massachusetts 02138, USA*
[30]*Universität Heidelberg, Physikalisches Institut, Philosophenweg 12, D-69120 Heidelberg, Germany*

[31]*Humboldt-Universität zu Berlin, Institut für Physik, Newtonstr. 15, D-12489 Berlin, Germany*
[32]*Imperial College London, London, SW7 2AZ, United Kingdom*
[33]*University of Iowa, Iowa City, Iowa 52242, USA*
[34]*Iowa State University, Ames, Iowa 50011-3160, USA*
[35]*Johns Hopkins University, Baltimore, Maryland 21218, USA*
[36]*Universität Karlsruhe, Institut für Experimentelle Kernphysik, D-76021 Karlsruhe, Germany*
[37]*Laboratoire de l'Accélérateur Linéaire, IN2P3/CNRS et Université Paris-Sud 11, Centre Scientifique d'Orsay, B. P. 34, F-91898 Orsay Cedex, France*
[38]*Lawrence Livermore National Laboratory, Livermore, California 94550, USA*
[39]*University of Liverpool, Liverpool L69 7ZE, United Kingdom*
[40]*Queen Mary, University of London, London, E1 4NS, United Kingdom*
[41]*University of London, Royal Holloway and Bedford New College, Egham, Surrey TW20 0EX, United Kingdom*
[42]*University of Louisville, Louisville, Kentucky 40292, USA*
[43]*University of Manchester, Manchester M13 9PL, United Kingdom*
[44]*University of Maryland, College Park, Maryland 20742, USA*
[45]*University of Massachusetts, Amherst, Massachusetts 01003, USA*
[46]*Massachusetts Institute of Technology, Laboratory for Nuclear Science, Cambridge, Massachusetts 02139, USA*
[47]*McGill University, Montréal, Québec, Canada H3A 2T8*
[48a]*INFN Sezione di Milano, I-20133 Milano, Italy*
[48b]*Dipartimento di Fisica, Università di Milano, I-20133 Milano, Italy*
[49]*University of Mississippi, University, Mississippi 38677, USA*
[50]*Université de Montréal, Physique des Particules, Montréal, Québec, Canada H3C 3J7*
[51]*Mount Holyoke College, South Hadley, Massachusetts 01075, USA*
[52a]*INFN Sezione di Napoli, I-80126 Napoli, Italy*
[52b]*Dipartimento di Scienze Fisiche, Università di Napoli Federico II, I-80126 Napoli, Italy*
[53]*NIKHEF, National Institute for Nuclear Physics and High Energy Physics, NL-1009 DB Amsterdam, The Netherlands*
[54]*University of Notre Dame, Notre Dame, Indiana 46556, USA*
[55]*Ohio State University, Columbus, Ohio 43210, USA*
[56]*University of Oregon, Eugene, Oregon 97403, USA*
[57a]*INFN Sezione di Padova, I-35131 Padova, Italy*
[57b]*Dipartimento di Fisica, Università di Padova, I-35131 Padova, Italy*
[58]*Laboratoire de Physique Nucléaire et de Hautes Energies, IN2P3/CNRS, Université Pierre et Marie Curie-Paris6, Université Denis Diderot-Paris7, F-75252 Paris, France*
[59]*University of Pennsylvania, Philadelphia, Pennsylvania 19104, USA*
[60a]*INFN Sezione di Perugia, I-06100 Perugia, Italy*
[60b]*Dipartimento di Fisica, Università di Perugia, I-06100 Perugia, Italy*
[61a]*INFN Sezione di Pisa, I-56127 Pisa, Italy*
[61b]*Dipartimento di Fisica, Università di Pisa, I-56127 Pisa, Italy*
[61c]*Scuola Normale Superiore di Pisa, I-56127 Pisa, Italy*
[62]*Princeton University, Princeton, New Jersey 08544, USA*
[63a]*INFN Sezione di Roma, I-00185 Roma, Italy*
[63b]*Dipartimento di Fisica, Università di Roma La Sapienza, I-00185 Roma, Italy*
[64]*Universität Rostock, D-18051 Rostock, Germany*
[65]*Rutherford Appleton Laboratory, Chilton, Didcot, Oxon, OX11 0QX, United Kingdom*
[66]*DSM/Irfu, CEA/Saclay, F-91191 Gif-sur-Yvette Cedex, France*
[67]*University of South Carolina, Columbia, South Carolina 29208, USA*
[68]*Stanford Linear Accelerator Center, Stanford, California 94309, USA*
[69]*Stanford University, Stanford, California 94305-4060, USA*
[70]*State University of New York, Albany, New York 12222, USA*
[71]*University of Tennessee, Knoxville, Tennessee 37996, USA*
[72]*University of Texas at Austin, Austin, Texas 78712, USA*
[73]*University of Texas at Dallas, Richardson, Texas 75083, USA*

[*]Deceased.
[+]Now at Temple University, Philadelphia, PA 19122, USA.
[‡]Now at Tel Aviv University, Tel Aviv, 69978, Israel.
[§]Also with Università di Perugia, Dipartimento di Fisica, Perugia, Italy.
[‖]Also with Università di Roma La Sapienza, I-00185 Roma, Italy.
[¶]Now at University of South Alabama, Mobile, AL 36688, USA.
[**]Also with Università di Sassari, Sassari, Italy.

[74a]*INFN Sezione di Torino, I-10125 Torino, Italy*
[74b]*Dipartimento di Fisica Sperimentale, Università di Torino, I-10125 Torino, Italy*
[75a]*INFN Sezione di Trieste, I-34127 Trieste, Italy*
[75b]*Dipartimento di Fisica, Università di Trieste, I-34127 Trieste, Italy*
[76]*IFIC, Universitat de Valencia-CSIC, E-46071 Valencia, Spain*
[77]*University of Victoria, Victoria, British Columbia, Canada V8W 3P6*
[78]*Department of Physics, University of Warwick, Coventry CV4 7AL, United Kingdom*
[79]*University of Wisconsin, Madison, Wisconsin 53706, USA*
(Received 9 August 2008; published 1 December 2008)

We present branching fraction measurements for the radiative decays $B^+ \to \rho^+\gamma$, $B^0 \to \rho^0\gamma$, and $B^0 \to \omega\gamma$. The analysis is based on a data sample of 465×10^6 $B\bar{B}$ events collected with the *BABAR* detector at the PEP-II asymmetric-energy B Factory located at the Stanford Linear Accelerator Center. We find $\mathcal{B}(B^+ \to \rho^+\gamma) = (1.20^{+0.42}_{-0.37} \pm 0.20) \times 10^{-6}$, $\mathcal{B}(B^0 \to \rho^0\gamma) = (0.97^{+0.24}_{-0.22} \pm 0.06) \times 10^{-6}$, and a 90% C.L. upper limit $\mathcal{B}(B^0 \to \omega\gamma) < 0.9 \times 10^{-6}$, where the first error is statistical and the second is systematic. We also measure the isospin-violating quantity $\Gamma(B^+ \to \rho^+\gamma)/2\Gamma(B^0 \to \rho^0\gamma) - 1 = -0.43^{+0.25}_{-0.22} \pm 0.10$.

DOI: 10.1103/PhysRevD.78.112001 PACS numbers: 12.15.Hh, 13.25.Hw

I. INTRODUCTION

Within the standard model (SM), the radiative decays $B^+ \to \rho^+\gamma$, $B^0 \to \rho^0\gamma$, and $B^0 \to \omega\gamma$[1] proceed mainly through a $b \to d\gamma$ electroweak penguin amplitude with a virtual top quark in the loop. Hence, the decay rates depend on the magnitude of the Cabibbo-Kobayashi-Maskawa (CKM) matrix element V_{td}. The branching fraction results from recent next-to-leading order calculations are listed in Table I. While these exclusive decay rates have a large theoretical uncertainty dominated by the imprecise knowledge of the form factors, some of this uncertainty cancels in the ratio of $B \to \rho(\omega)\gamma$ to $B \to K^*\gamma$ branching fractions. This ratio provides a constraint on the ratio of the CKM matrix elements $|V_{td}/V_{ts}|$, which can also be obtained from the ratio of B_d and B_s mixing frequencies [4]. Physics beyond the SM could affect differently $B \to \rho(\omega)\gamma$ and B_d/B_s mixing, and hence create inconsistencies between the results obtained from the two methods.

The ratio of $B \to \rho(\omega)\gamma$ to $B \to K^*\gamma$ branching fractions is related to $|V_{td}/V_{ts}|$ [5] via

$$\frac{\mathcal{B}[B \to \rho(\omega)\gamma]}{\mathcal{B}(B \to K^*\gamma)} = S\left|\frac{V_{td}}{V_{ts}}\right|^2\left(\frac{1 - m^2_{\rho(\omega)}/m^2_B}{1 - m^2_{K^*}/m^2_B}\right)^3 \zeta^2_{\rho(\omega)} \times [1 + \Delta R_{\rho(\omega)}]. \quad (1)$$

The coefficient S is 1 for ρ^+ and $\frac{1}{2}$ for ρ^0 or ω, m is the particle mass, $\zeta_{\rho(\omega)}$ is the ratio of the form factors for the decays $B \to \rho(\omega)\gamma$ and $B \to K^*\gamma$, and $\Delta R_{\rho(\omega)}$ accounts for differences in decay dynamics, including weak annihilation contributions. The precision of the $|V_{td}/V_{ts}|$ determination can be improved by using an average branching fraction for $B \to \rho(\omega)\gamma$ decays. Within the SM, the isospin asymmetry between $B^+ \to \rho^+\gamma$ and $B^0 \to \rho^0\gamma$ is dominated by weak annihilation contributions, and is expected to be small; on the other hand, the asymmetry between $B^0 \to \rho^0\gamma$ and $B^0 \to \omega\gamma$ can be sizable, due to the difference in the form factors [1,3].

We report an updated study of the decays $B^+ \to \rho^+\gamma$, $B^0 \to \rho^0\gamma$, and $B^0 \to \omega\gamma$ based on 465×10^6 $B\bar{B}$ events, corresponding to an integrated luminosity of 423 fb^{-1}, a data sample 25% larger than that used in our previous publication [6]. In addition, we reduce backgrounds considerably by using a multivariate algorithm based on bootstrap-aggregated (bagged) decision trees (BDTs) [7] and additional discriminating variables to separate signal from background.

II. THE *BABAR* DETECTOR AND DATA SET

The data sample is collected with the *BABAR* detector at the PEP-II asymmetric-energy e^+e^- storage ring at a center-of-mass (CM) energy near $\sqrt{s} = 10.58$ GeV, corresponding to the $\Upsilon(4S)$ resonance (on resonance). Charged particle trajectories and energy loss (dE/dx) are measured with a five-layer silicon vertex tracker (SVT) and a 40-layer drift chamber (DCH) in a 1.5 T magnetic field. Photons and electrons are detected in a CsI(Tl) crystal electromagnetic calorimeter (EMC) with photon energy resolution $\sigma_E/E = 0.023(E/\text{GeV})^{-1/4} \oplus 0.019$. A ring-imaging Cherenkov detector based on the detection of internally reflected Cherenkov light (DIRC) provides information for charged particle identification. The K-π

TABLE I. Recent predictions of the branching fractions.

Mode	Branching fraction ($\times 10^{-6}$)		
	Reference [1]	Reference [2]	Reference [3]
$B^+ \to \rho^+\gamma$	1.41 ± 0.27	$1.58^{+0.53}_{-0.46}$	1.16 ± 0.26
$B^0 \to \rho^0\gamma$	0.69 ± 0.12	$0.76^{+0.26}_{-0.23}$	0.55 ± 0.13
$B^0 \to \omega\gamma$	0.55 ± 0.09		0.44 ± 0.10

[1]Charge conjugate modes are implied throughout.

separation in the DIRC is above 4σ at laboratory momenta up to 3 GeV/c. In order to identify muons, the magnetic flux return is instrumented with resistive plate chambers and limited streamer tubes. A detailed description of the detector can be found elsewhere [8].

We use a GEANT4-based [9] Monte Carlo (MC) simulation to model the *BABAR* detector response, taking into account the varying accelerator and detector conditions. Dedicated signal and background MC samples are used to optimize selection criteria, to obtain signal efficiencies, and to validate the analysis. Data control samples, including 41 fb^{-1} of data collected about 40 MeV below the $B\bar{B}$ production threshold (off resonance), are used to study backgrounds coming from continuum $e^+e^- \to q\bar{q}$, with $q = u, d, s, c$.

III. EVENT RECONSTRUCTION AND BACKGROUND SUPPRESSION

The decays $B \to \rho(\omega)\gamma$ are reconstructed by combining a high-energy photon with a vector meson reconstructed in the decay modes $\rho^+ \to \pi^+\pi^0$, $\rho^0 \to \pi^+\pi^-$, and $\omega \to \pi^+\pi^-\pi^0$. The dominant source of background is coming from continuum events that contain a high-energy photon from π^0 or η decays or from initial-state radiation (ISR). There are also significant backgrounds from B meson decays. The decays $B \to K^*\gamma$, $K^* \to K\pi$ can mimic the signal when the kaon is misidentified as a pion. Decays of $B \to (\rho/\omega)(\pi^0/\eta)$ with a high-energy photon from the π^0 or η decay also mimic the signal. In addition, there are other B backgrounds originating mainly from $B \to X_s\gamma$ and $B \to X(\pi^0/\eta)$ decays.

The event selection and background suppression are performed in two steps. We apply a set of loose selection criteria to select well-measured photons and charged pions and to reject background events that are kinematically very different from the signal events. For events that pass the loose event selection criteria, we then use the BDT technique to further reduce background.

A. Loose selection

We reduce background contributions from continuum processes by considering only events for which the ratio R_2 of second-to-zeroth Fox-Wolfram moments [10], calculated using the momenta of all charged and neutral particles in the event, is less than 0.7.

A photon candidate is identified as a cluster of energy deposited in contiguous EMC crystals, and not associated with any charged track. The high-energy photon must have energy $1.5 < E_\gamma < 4.4$ GeV in the laboratory frame and $1.5 < E^*_\gamma < 3.5$ GeV in the CM frame, be well contained within the EMC acceptance with polar angle $-0.74 < \cos\theta < 0.93$, and be isolated by at least 25 cm at the entrance of the EMC from any other photon candidate or charged track. The distribution of the energy deposition is required to be consistent with that of a photon shower.

Charged-pion candidates are selected from well-reconstructed tracks that have at least 12 DCH hits used in the track fit and a minimum momentum transverse to the beam direction of 100 MeV/c. The tracks are required to originate near the interaction point (IP): the distance of closest approach to the IP must be less than 10 cm along the beam direction and less than 2 cm in the plane perpendicular to the beam direction. The $\pi^\pm$ identification is based on a likelihood L_i computed for particle hypothesis $i(= \pi, K, p)$ using dE/dx measured in the SVT and DCH and the information of Cherenkov photons detected by the DIRC. The selection criteria are optimized to reject charged kaons produced in $B \to K^*\gamma$ decays. The pion candidates in $B^0 \to \omega\gamma$ must have $L_K/(L_K + L_\pi) < 0.5$ and $L_p/(L_p + L_\pi) < 0.98$ and must not be consistent with being an electron. The pion candidates in $B \to \rho\gamma$ must have $L_K/(L_K + L_\pi) < 0.2$ and $L_p/(L_p + L_\pi) < 0.5$ and must not be consistent with either an electron or a muon candidate hypothesis; in addition, for all candidates with laboratory momenta above 0.6 GeV/c, the number of photons observed in the DIRC is required to be consistent with the number that is expected for the pion hypothesis. The performance of the pion identification requirements is evaluated with the decay $D^{*+} \to D^0(\to K^-\pi^+)\pi^+$, which provides a large, clean sample of $\pi^\pm$ and $K^\pm$. Using the results shown in Fig. 1, we find that the pion identification requirement retains 85% of the pions from $B \to \rho\gamma$ decays and rejects 99% of the kaons from $B \to K^*\gamma$ decays.

We form π^0 candidates from pairs of photons with energies greater than 50 MeV in the laboratory frame and an invariant mass $m_{\gamma\gamma}$ in the range 115–150 MeV/c^2. We combine the identified pions into vector-meson candidates requiring $630 < m_{\pi^+\pi^-} < 960$MeV/$c^2$, $640 < m_{\pi^+\pi^0} < 930$ MeV/c^2, and $760 < m_{\pi^+\pi^-\pi^0} < 790$ MeV/c^2 for ρ^0, ρ^+, and ω, respectively. The charged-pion pairs are required to originate from a common vertex.

The photon and ρ/ω candidates are combined to form the B meson candidates. We define $\Delta E \equiv E^*_B - \sqrt{s}/2$, where $E^*_B = E^*_{\rho/\omega} + E^*_\gamma$ is the CM energy of the B meson candidate. The ΔE distributions of signal events are expected to peak near zero with a resolution of about 50 MeV dominated by the photon energy resolution, and to have a tail in the negative region due to photon energy loss in the detector. We also define the beam-energy-substituted mass $m_{\rm ES} \equiv \sqrt{s/4 - \mathbf{p}^{*2}_B}$, where $\mathbf{p}^*_B$ is the CM momentum of the B candidate modified by scaling the photon momentum so that $E^*_{\rho/\omega} + E'^*_\gamma - \sqrt{s}/2 = 0$. This procedure improves the $m_{\rm ES}$ resolution for the signal events in the ΔE negative tail. Signal events are expected to have an $m_{\rm ES}$ distribution centered at the mass of the B meson $m_{\rm B}$ with a resolution of 3 MeV/c^2. We consider candidates with $m_{\rm ES} > 5.22$ GeV/c^2 and $-0.3 < \Delta E < 0.3$ GeV for further analysis. This region includes sidebands that allow the continuum background yields to be extracted from a fit to the data.

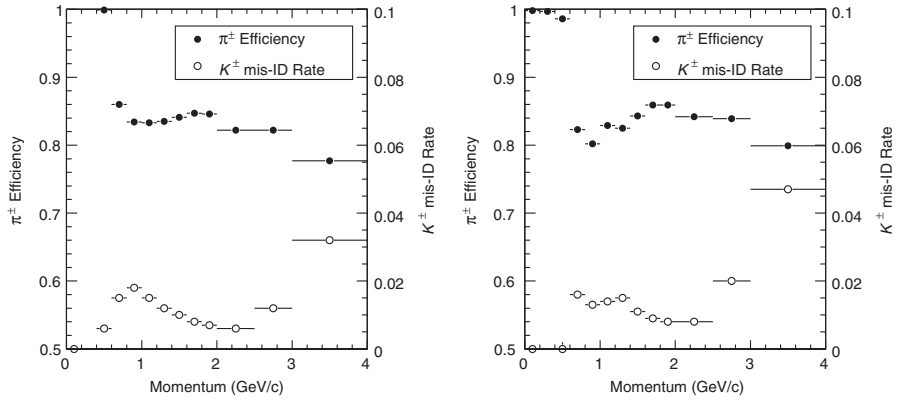

FIG. 1. Performance of the charged-pion identification requirement applied to $B \to \rho\gamma$ decays, evaluated using the D^* control sample. Filled circles are for $\pi^\pm$ efficiency and use the left-hand scale. Open circles are for $K^\pm$ misidentification and use the right-hand scale. The plot on the left shows results for continuum MC events and the plot on the right shows results for data.

The signal efficiencies for the loose selection described above are 22% for $B^+ \to \rho^+\gamma$, 25% for $B^0 \to \rho^0\gamma$, and 17% for $B^0 \to \omega\gamma$.

B. Bagged decision tree

The bagged decision trees are trained separately for the $B^+ \to \rho^+\gamma$, $B^0 \to \rho^0\gamma$, and $B^0 \to \omega\gamma$ channels with MC simulated signal and background samples of about 60 000 and 90 000 events, respectively, and then validated with independent samples of the same size. The background sample consists of a $B\bar{B}$ MC sample that is about 3 times larger than the data and of a continuum MC sample that is about 1.5 times larger. For the input classifiers, we choose approximately 60 event quantities that characterize the kinematics of the π^0 candidates, the high-energy photon, the vector meson, the B meson, and the rest of the event (ROE), which are the particles that are not used to reconstruct the B candidate. These quantities all have distributions that agree well between off-resonance data and continuum MC events.

To reduce combinatorial background in the reconstructed π^0 candidates, we use in the BDT the invariant mass $m_{\gamma\gamma}$ and $\cos\theta_{\gamma\gamma}$, the cosine of the opening angle between the photons in the laboratory frame.

We associate the high-energy photon candidate γ with each of the other photons γ' in the event and calculate the likelihood ratio

$$\mathcal{LR}_i = \frac{\mathcal{P}(m_{\gamma\gamma'}, E_{\gamma'}|i)}{\mathcal{P}(m_{\gamma\gamma'}, E_{\gamma'}|\text{signal}) + \mathcal{P}(m_{\gamma\gamma'}, E_{\gamma'}|i)}, \qquad (2)$$

where $i = \pi^0$, η and $\mathcal{P}$ is the probability density function (PDF) defined in terms of the energy of the second photon in the laboratory frame $E_{\gamma'}$ and the invariant mass of the pair $m_{\gamma\gamma'}$. The PDFs are determined from simulated signal and continuum background events. The likelihood ratios $\mathcal{LR}_{\pi^0}$ and $\mathcal{LR}_\eta$ are used in the BDT to reject high-energy photons from π^0 and η decays.

To reject background events from $B \to \rho(\pi^0/\eta)$ and $B \to \omega(\pi^0/\eta)$, we also use the vector-meson helicity angle θ_H, which is defined as the angle between the B momentum vector and the π^+ track calculated in the ρ rest frame for a ρ meson, or the angle between the B momentum vector and the normal to the ω decay plane for an ω meson. This variable is useful because in signal events the vector meson is transversely polarized, while in the background events it is longitudinally polarized.

Variables used in the BDT to reduce continuum background include R_2, the significance of the separation of the two B vertices along the beam axis ($S_{\Delta z}$), the polar angle of the B candidate momentum in the CM frame with respect to the beam axis (θ_B^*), and R_2', which is R_2 in the frame recoiling against the photon momentum. We compute the moments $M_i \equiv \sum_j p_j^* \cdot |\cos\theta_j^*|^i / \sum_j p_j^*$ with $i = 1, 2, 3$, where p_j^* is the momentum of each particle j in the ROE and θ_j^* is the angle of the momentum with respect to an axis. We use the M_i with respect to the photon direction and the ROE thrust axis. We also include flavor-tagging variables [11] to exploit the differences in lepton and kaon production between background and B decays.

While we find that all the variables contribute to the sensitivity of the analysis, the most effective ones are $S_{\Delta z}$, $\cos\theta_{\gamma\gamma}$, R_2, $\cos\theta_B^*$, M_3 with respect to the photon direction, the missing mass of the ROE, $\cos\theta_H$, and $\mathcal{LR}_{\pi^0,\eta}$. The distribution of the BDT output for the decay $B^0 \to \rho^0\gamma$ is shown in Fig. 2. We require the BDT output to be greater than 0.94 (0.93) for $B \to \rho\gamma$ ($B^0 \to \omega\gamma$). These selection requirements have been optimized for maximum statistical signal significance with assumed signal branching fractions of 1.0×10^{-6} and 0.5×10^{-6} for the charged and neutral modes, respectively. The signal significance is determined from a fit described in the next section. For the signal events that pass the loose selection criteria, the BDT requirements have an efficiency of 19% for $B^+ \to \rho^+\gamma$, 31% for $B^0 \to \rho^0\gamma$, and 34% for $B^0 \to \omega\gamma$.

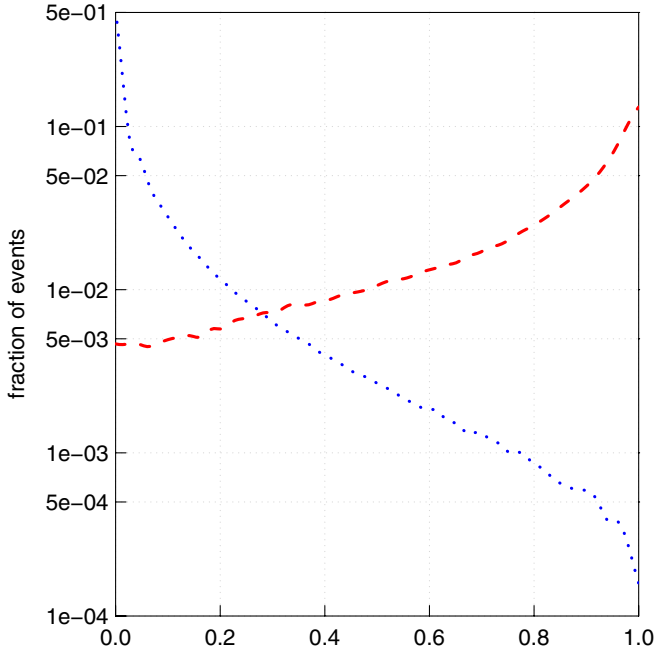

FIG. 2 (color online). Distributions of the BDT output for $B^0 \to \rho^0\gamma$ in signal (dashed line) and background (dotted line) MC samples. The distributions are normalized to the same area.

In events where multiple candidates are present, we select the one with the reconstructed vector-meson mass closest to the nominal mass. This criterion is chosen because the mass of the vector meson is found to be uncorrelated with the variables used in the fit. After applying all the selection criteria described above to signal MC samples, we find signal efficiencies of 4.2% for $B^+ \to \rho^+\gamma$, 7.7% for $B^0 \to \rho^0\gamma$, and 5.2% for $B^0 \to \omega\gamma$ [taking into account the branching fraction $\mathcal{B}(\omega \to \pi^+\pi^-\pi^0) = 0.892 \pm 0.007$ [12]], while backgrounds are reduced by $O(10^{-5})$.

IV. MAXIMUM LIKELIHOOD FIT

We determine signal yields from an unbinned maximum likelihood fit to $m_{\rm ES}$ and ΔE. The likelihood function for a signal mode k ($= \rho^+\gamma$, $\rho^0\gamma$, $\omega\gamma$) with a sample of N_k events is defined as

$$\mathcal{L}_k = \exp\Big(-\sum_{i=1}^{N_{\rm hyp}} n_i\Big)\Big[\prod_{j=1}^{N_k}\Big(\sum_{i=1}^{N_{\rm hyp}} n_i \mathcal{P}_i(\vec{x}_j;\vec{\alpha}_i)\Big)\Big], \quad (3)$$

where $N_{\rm hyp}$ is the number of event hypotheses, and n_i is the yield for each. For $B^0 \to \omega\gamma$, three event hypotheses are considered: signal, continuum background, and combinatorial B backgrounds. For $B^0 \to \rho^0\gamma$, a $B^0 \to K^{*0}\gamma$ background hypothesis is also included, while for $B^+ \to \rho^+\gamma$, a combined $B^+ \to K^{*+}\gamma/\rho^+\pi^0$ hypothesis is included. Since the correlations between $m_{\rm ES}$ and ΔE are found to be negligible in MC event samples, we define the probability density function $\mathcal{P}_i(\vec{x}_j;\vec{\alpha}_i)$ as the product of individual PDFs for each observable $x_j = m_{\rm ES}$, ΔE, given the set of parameters $\vec{\alpha}_i$.

The individual PDFs are determined from fits to dedicated MC event samples. The signal $m_{\rm ES}$ PDFs are parametrized by a Crystal Ball (CB) function [13] and the ΔE PDFs are parametrized as

$$f(\Delta E) \propto \exp\Big(\frac{-(\Delta E-\mu)^2}{2\sigma_{L,R}^2 + \alpha_{L,R}(\Delta E-\mu)^2}\Big), \quad (4)$$

where μ is the peak position of the distribution, σ_L and σ_R are the widths on the left and right of the peak, and α_L and α_R are measures of the tails on the left and right of the peak, respectively. The peak positions and widths of the signal $m_{\rm ES}$ and ΔE PDFs are corrected for the observed difference between data and MC samples of $B \to K^*\gamma$ decays. The PDFs for the remaining $B^0 \to K^{*0}\gamma$ and combined $B^+ \to K^{*+}\gamma/B^+ \to \rho^+\pi^0$ backgrounds are determined from dedicated MC samples that are 100 times larger than the data. These PDFs are described by a CB function for $m_{\rm ES}$ with a peak position the same as that of the signal PDF—but with a much larger width—and a CB function for ΔE with a peak position near -80 MeV. The negative ΔE peak position is due either to a kaon misidentified as a pion in $B \to K^*\gamma$ or to a single missing photon in $B^+ \to \rho^+\pi^0$. The $m_{\rm ES}$ and ΔE PDFs for all other B backgrounds are determined from the $B\bar{B}$ MC sample. The $m_{\rm ES}$ spectra peak slightly in the signal region, and therefore are parametrized by a CB function, while the ΔE spectra are parametrized by an exponential function. The continuum $m_{\rm ES}$ and ΔE PDFs are parametrized by an ARGUS threshold function [14] and a first order polynomial, respectively.

The fit to the data determines the signal yield $n_{\rm sig}$, the continuum yield, and the shape parameters of the continuum PDFs. The shape parameters of the signal and B background PDFs are fixed in the fit. The relative yield between the peaking and the other B backgrounds is fixed to the value obtained from known branching fractions [12] and selection efficiencies determined from MC event samples. The overall yields of the B backgrounds are also fixed. All fixed parameters are later varied to evaluate systematic errors in $n_{\rm sig}$.

We validate the fitting procedure using ensembles of signal and background events, with signal contributions of zero, 1, and 2 times the rate expected from previous measurements of the $\rho^+\gamma$, $\rho^0\gamma$, and $\omega\gamma$ branching fractions. Two types of ensembles are produced: one with both signal and background events generated using the PDFs described above, and the other with signal events randomly sampled from the GEANT4 MC events and background events generated using the corresponding PDFs. No bias is found in the fit to these event samples.

Figure 3 shows the data points and the projections of the fit results for ΔE and $m_{\rm ES}$ separately for each decay mode.

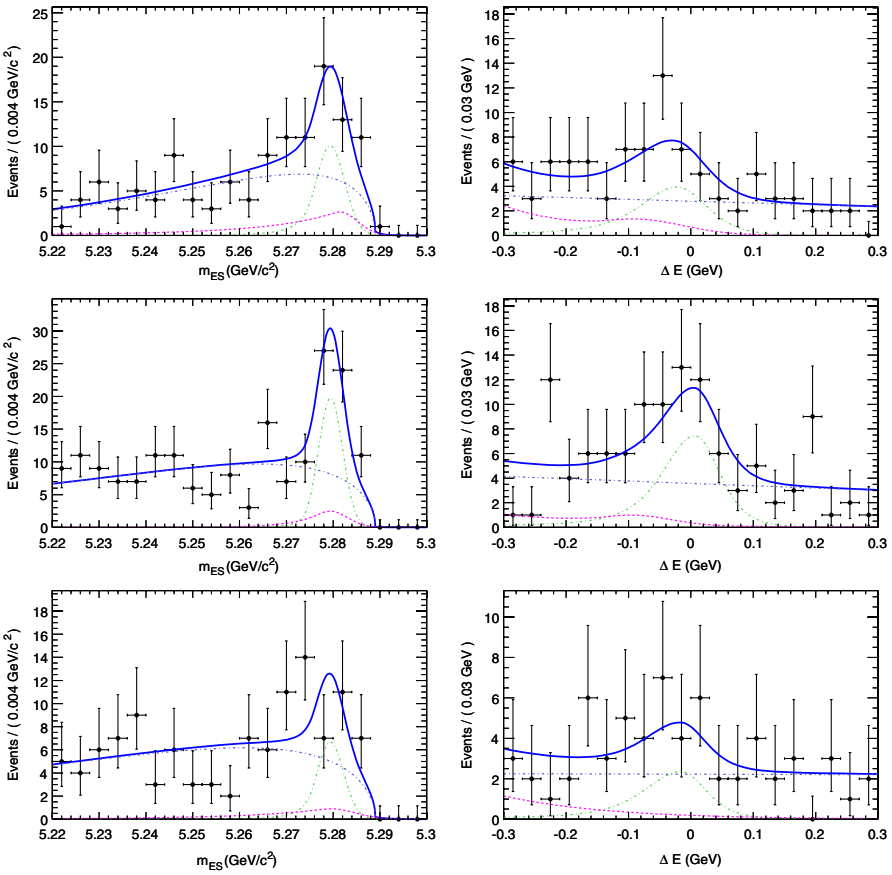

FIG. 3 (color online). ΔE and $m_{\rm ES}$ projections of the fits for the decay modes $B^+ \to \rho^+\gamma$ (top panels), $B^0 \to \rho^0\gamma$ (middle panels), and $B^0 \to \omega\gamma$ (bottom panels). For illustrative purposes only, these plots are made by requiring $-0.2 < \Delta E < 0.1$ GeV for the $m_{\rm ES}$ projections and $m_{\rm ES} > 5.27$ GeV$/c^2$ for the ΔE projections. The points are data, the solid line is the fit result, the dashed line is the sum of B backgrounds, and the dash-dotted and dotted lines are the contributions from continuum background and signal, respectively.

The signal yields are reported in Table II. The significance is computed as $\sqrt{2\Delta \ln \mathcal{L}}$, where $\Delta \ln \mathcal{L}$ is the log-likelihood difference between the best fit and the null-signal hypothesis. To take into account the systematic error in $n_{\rm sig}$, the likelihood function is convolved with a Gaussian distribution that has a width equal to the systematic error.

TABLE II. The signal yield $n_{\rm sig}$, significance Σ in standard deviations including the systematic error in $n_{\rm sig}$, efficiency ϵ, and branching fraction $\mathcal{B}$ for each mode. The first error is statistical and the second is systematic. The branching fractions for $B \to (\rho/\omega)\gamma$ and $B \to \rho\gamma$ are obtained with the assumption of isospin and SU(3)$_{\rm F}$ symmetries; see Sec. VI.

Mode	$n_{\rm sig}$	Σ	$\epsilon(\%)$	$\mathcal{B}(10^{-6})$
$B^+ \to \rho^+\gamma$	$23.3^{+8.1}_{-7.3} \pm 3.1$	3.2σ	4.2	$1.20^{+0.42}_{-0.37} \pm 0.20$
$B^0 \to \rho^0\gamma$	$34.9^{+8.6}_{-7.9} \pm 1.2$	5.4σ	7.7	$0.97^{+0.24}_{-0.22} \pm 0.06$
$B^0 \to \omega\gamma$	$12.4^{+6.6}_{-5.7} \pm 2.0$	2.2σ	5.2	$0.50^{+0.27}_{-0.23} \pm 0.09$
$B \to (\rho/\omega)\gamma$		6.5σ		$1.63^{+0.30}_{-0.28} \pm 0.16$
$B \to \rho\gamma$		6.0σ		$1.73^{+0.34}_{-0.32} \pm 0.17$

V. SYSTEMATIC UNCERTAINTIES

Table III gives the contributions to the systematic uncertainties. The systematic error affecting the signal efficiency includes uncertainties on tracking, particle identification, γ and π^0 reconstruction, and BDT selection. The modeling of signal and background in the fit contributes to the uncertainties on the signal yields.

TABLE III. Fractional systematic errors (in %) of the measured branching fractions.

Source of error	$\rho^+\gamma$	$\rho^0\gamma$	$\omega\gamma$	$\rho\gamma$	$(\rho/\omega)\gamma$
Tracking efficiency	0.4	0.4	0.4	0.4	0.4
Particle identification	1.0	2.0	1.0	1.4	1.2
Photon selection	2.8	2.8	2.8	2.8	2.8
π^0 reconstruction	3.0	$\cdots$	3.0	1.7	2.0
BDT efficiency	9.3	4.2	5.1	7.0	7.5
Signal model	7.1	2.1	16.3	3.0	3.0
Background model	10.9	2.8	2.7	4.3	3.6
$B\bar{B}$ counting	1.1	1.1	1.1	1.1	1.1
$\mathcal{B}(\omega \to \pi^+\pi^-\pi^0)$	$\cdots$	$\cdots$	0.8	$\cdots$	0.1
Sum in quadrature	16.7	6.6	17.9	9.5	9.5

The errors in BDT selections are determined from a control sample of the decay $B^0 \to K^{*0}(\to K^+\pi^-)\gamma$ for the ρ^0 mode and a sample of $B^+ \to K^{*+}(\to K^+\pi^0)\gamma$ for the ρ^+ and ω modes. These $B \to K^*\gamma$ decays are kinematically similar to $B \to (\rho/\omega)\gamma$ decays. The events are required to pass all applicable loose selection criteria, except the pion identification requirements. We also require the invariant mass $0.80 < m_{K^+\pi^-} < 1.0$ GeV/c^2 and $0.82 < m_{K^+\pi^0} < 0.96$ GeV/c^2. The BDT output classifiers are computed from the decision trees trained for the corresponding signal modes. The differences in the BDT selection efficiencies between the $B \to K^*\gamma$ data and MC samples are used to correct the signal efficiencies. The efficiency correction factor is 0.88 ± 0.09 for $B^+ \to \rho^+\gamma$, 0.91 ± 0.04 for $B^0 \to \rho^0\gamma$, and 0.90 ± 0.05 for $B^0 \to \omega\gamma$. The uncertainty of the correction is taken as the systematic error. The large BDT systematic error for the decay $B^+ \to \rho^+\gamma$ is due to the limited size of the $B^+ \to K^{*+}(\to K^+\pi^0)\gamma$ sample. As a means of validating the BDT technique, we apply the same analysis technique to the $B \to K^*\gamma$ data control samples and measure the branching fractions for $B \to K^*\gamma$. The results are consistent with the world averages [12].

The error in the pion identification requirements is estimated using the D^* control sample as shown in Fig. 1. Based on the difference of a momentum-weighted efficiency between the continuum MC sample and data, a 1% systematic error per charged pion is assigned to the $B \to \rho\gamma$ decays. The MC sample is in better agreement with data for the looser pion identification criteria applied to $B^0 \to \omega\gamma$, and a 0.5% error per charged pion is assigned. The uncertainties from tracking, π^0 reconstruction, and photon selection are also determined from suitable independent data control samples.

To estimate the uncertainty related to the modeling of the signal and background, we vary the parameters of the PDFs that are fixed in the fit within their errors. We vary the relative and absolute normalizations of B background components that are fixed in the fit based on a kaon misidentification study using the D^* control sample as shown in Fig. 1. We find that the difference in the momentum-weighted kaon misidentification rates between the data and MC samples is 23%, and we conservatively vary the $B \to K^*\gamma$ background yield by 30%. The effect of the uncertainty of $\mathcal{B}(B^+ \to \rho^+\pi^0)$ [12] is also considered for the decay $B^+ \to \rho^+\gamma$. For all the variations, the corresponding changes in the extracted signal yield are taken as systematic uncertainties, which are then combined, taking into account correlations. The error on background modeling for $B^+ \to \rho^+\gamma$ is dominated by uncertainties in B background PDFs.

VI. RESULTS

To calculate the branching fractions from the measured signal yields, we assume $\mathcal{B}(\Upsilon(4S) \to B^0\bar{B}^0) = \mathcal{B}(\Upsilon(4S) \to B^+B^-) = 0.5$. The results are listed in Table II. For $B^0 \to \omega\gamma$, we also compute the 90% C.L. upper limit $\mathcal{B}(B^0 \to \omega\gamma) < 0.9 \times 10^{-6}$ using a Bayesian technique, assuming a prior that is flat in the branching fraction and taking into account the systematic uncertainty.

We test the hypothesis of isospin symmetry by measuring the quantity

$$\Delta_\rho = \frac{\Gamma(B^+ \to \rho^+\gamma)}{2\Gamma(B^0 \to \rho^0\gamma)} - 1 = -0.43^{+0.25}_{-0.22} \pm 0.10.$$

Most theoretical calculations [1–3,15] predict small Δ_ρ. For example, the estimate in Ref. [3] is -0.05 ± 0.03 for $\gamma = 60°$ and -0.10 ± 0.02 for $\gamma = 70°$, where γ is the phase of V^*_{ub}. Our result is consistent with these predictions within the large experimental errors. However, it is worth noting that a recent calculation [16] indicated that nonperturbative charming penguin contributions can accommodate large Δ_ρ. We also measure the $SU(3)_F$-violating quantity

$$\Delta_\omega = \frac{\Gamma(B^0 \to \omega\gamma)}{\Gamma(B^0 \to \rho^0\gamma)} - 1 = -0.49^{+0.30}_{-0.27} \pm 0.10,$$

which is consistent with the theoretical calculations.

We extract average branching fractions using a simultaneous fit to all the relevant decay modes with the constraints on the widths of the decay modes: $\Gamma_{B^+\to\rho^+\gamma} = 2\Gamma_{B^0\to\rho^0\gamma} = 2\Gamma_{B^0\to\omega\gamma}$. The average branching fractions are defined as

$$\mathcal{B}(B \to \rho\gamma) \equiv \frac{1}{2}\Big[\mathcal{B}(B^+ \to \rho^+\gamma) + 2\frac{\tau_{B^+}}{\tau_{B^0}}\mathcal{B}(B^0 \to \rho^0\gamma)\Big] \quad (5)$$

and

$$\mathcal{B}[B \to (\rho/\omega)\gamma] \equiv \frac{1}{2}\Big\{\mathcal{B}(B^+ \to \rho^+\gamma) + \frac{\tau_{B^+}}{\tau_{B^0}}[\mathcal{B}(B^0 \to \rho^0\gamma) + \mathcal{B}(B^0 \to \omega\gamma)]\Big\}, \quad (6)$$

where τ_{B^+}/τ_{B^0} is the measured ratio between the charged and neutral B meson lifetimes, for which the current world average is 1.071 ± 0.009 [12]. Our measurements of the individual branching fractions are consistent with this hypothesis, with a χ^2 of 2.3 for 2 degrees of freedom. We find

$$\mathcal{B}(B \to \rho\gamma) = (1.73^{+0.34}_{-0.32} \pm 0.17) \times 10^{-6},$$
$$\mathcal{B}[B \to (\rho/\omega)\gamma] = (1.63^{+0.30}_{-0.28} \pm 0.16) \times 10^{-6}.$$

Using the world average value of $\mathcal{B}(B^+ \to K^{*+}\gamma) = (4.03 \pm 0.26) \times 10^{-5}$, $\mathcal{B}(B^0 \to K^{*0}\gamma) = (4.01 \pm 0.2) \times 10^{-5}$ [12], and the isospin averaged branching fraction $\mathcal{B}(B \to K^*\gamma) = (4.16 \pm 0.17) \times 10^{-5}$, we calculate

$$R_{\rho^+} = \frac{\mathcal{B}(B^+ \to \rho^+\gamma)}{\mathcal{B}(B^+ \to K^{*+}\gamma)} = 0.030^{+0.012}_{-0.011},$$

$$R_{\rho^0} = \frac{\mathcal{B}(B^0 \to \rho^0\gamma)}{\mathcal{B}(B^0 \to K^{*0}\gamma)} = 0.024 \pm 0.006,$$

$$R_{\omega} = \frac{\mathcal{B}(B^0 \to \omega\gamma)}{\mathcal{B}(B^0 \to K^{*0}\gamma)} = 0.012^{+0.007}_{-0.006},$$

$$R_{\rho} = \frac{\mathcal{B}(B \to \rho\gamma)}{\mathcal{B}(B \to K^{*}\gamma)} = 0.042 \pm 0.009,$$

$$R_{\rho/\omega} = \frac{\mathcal{B}[B \to (\rho/\omega)\gamma]}{\mathcal{B}(B \to K^{*}\gamma)} = 0.039 \pm 0.008.$$

These ratios of branching fractions can be used to calculate $|V_{td}/V_{ts}|$ [3,5,17]. Following Eq. (1) and using $1/\zeta_\rho = 1.17 \pm 0.09$, $1/\zeta_\omega = 1.30 \pm 0.10$ [3], $\Delta R_{\rho^+} = 0.057^{+0.057}_{-0.055}$, $\Delta R_{\rho^0} = 0.006^{+0.046}_{-0.043}$, and $\Delta R_\omega = -0.002^{+0.046}_{-0.043}$ [1] , we obtain

$$|V_{td}/V_{ts}|_{\rho^+} = 0.198^{+0.039}_{-0.035} \pm 0.016,$$

$$|V_{td}/V_{ts}|_{\rho^0} = 0.254^{+0.033}_{-0.031} \pm 0.021,$$

$$|V_{td}/V_{ts}|_{\omega} = 0.202^{+0.058}_{-0.050} \pm 0.016,$$

where the first error is experimental and the second is theoretical. Using the average branching fractions and following Ref. [1], we obtain

$$|V_{td}/V_{ts}|_{\rho} = 0.235^{+0.026}_{-0.025} \pm 0.020,$$

$$|V_{td}/V_{ts}|_{\rho/\omega} = 0.233^{+0.025+0.022}_{-0.024-0.021}.$$

Similar values are found following Ref. [3]. These results are consistent with the value of this ratio, $0.208 \pm 0.002(\text{exp})^{+0.008}_{-0.006}(\text{theory})$ [12], obtained from the studies of B_d and B_s mixing by the CDF and D0 Collaborations.

VII. SUMMARY

We report the updated measurements of the branching fractions for the radiative decays $B^+ \to \rho^+\gamma$, $B^0 \to \rho^0\gamma$, and $B^0 \to \omega\gamma$,

$$\mathcal{B}(B^+ \to \rho^+\gamma) = (1.20^{+0.42}_{-0.37} \pm 0.20) \times 10^{-6},$$

$$\mathcal{B}(B^0 \to \rho^0\gamma) = (0.97^{+0.24}_{-0.22} \pm 0.06) \times 10^{-6},$$

$$\mathcal{B}(B^0 \to \omega\gamma) < 0.9 \times 10^{-6} (90\%\ \text{C.L.}).$$

We test the hypothesis of isospin symmetry by measuring the quantity $\Delta_\rho = -0.43^{+0.25}_{-0.22} \pm 0.10$. We also measure the averaged branching fractions $\mathcal{B}(B \to \rho\gamma) = (1.73^{+0.34}_{-0.32} \pm 0.17) \times 10^{-6}$ and $\mathcal{B}[B \to (\rho/\omega)\gamma] = (1.63^{+0.30}_{-0.28} \pm 0.16) \times 10^{-6}$. These results are in good agreement with, and supersede, the previous published *BABAR* measurement [6], which uses a subsample of the data used for this analysis. These results are also consistent with the measurements from Belle [18]. These branching fraction measurements are used to extract $|V_{td}/V_{ts}|$ in a way that is complementary to the approach using B mixing [4].

ACKNOWLEDGMENTS

We are grateful for the extraordinary contributions of our PEP-II2 colleagues in achieving the excellent luminosity and machine conditions that have made this work possible. The success of this project also relies critically on the expertise and dedication of the computing organizations that support *BABAR*. The collaborating institutions wish to thank SLAC for its support and the kind hospitality extended to them. This work is supported by the U.S. Department of Energy and National Science Foundation, the Natural Sciences and Engineering Research Council (Canada), the Commissariat à l'Energie Atomique and Institut National de Physique Nucléaire et de Physique des Particules (France), the Bundesministerium für Bildung und Forschung and Deutsche Forschungsgemeinschaft (Germany), the Istituto Nazionale di Fisica Nucleare (Italy), the Foundation for Fundamental Research on Matter (The Netherlands), the Research Council of Norway, the Ministry of Education and Science of the Russian Federation, Ministerio de Educación y Ciencia (Spain), and the Science and Technology Facilities Council (United Kingdom). Individuals have received support from the Marie-Curie IEF program (European Union) and the A. P. Sloan Foundation.

[1] A. Ali and A. Y. Parkhomenko, arXiv:hep-ph/0610149; updated analysis (to be published).
[2] S. W. Bosch and G. Buchalla, Nucl. Phys. **B621**, 459 (2002).
[3] P. Ball and R. Zwicky, J. High Energy Phys. 04 (2006) 046; P. Ball, G. Jones, and R. Zwicky, Phys. Rev. D **75**, 054004 (2007).
[4] A. Abulencia *et al.* (CDF Collaboration), Phys. Rev. Lett. **97**, 242003 (2006); V. Abazov *et al.* (D0 Collaboration), Phys. Rev. Lett. **97**, 021802 (2006).
[5] A. Ali and A. Y. Parkhomenko, Eur. Phys. J. C **23**, 89 (2002); A. Ali, E. Lunghi, and A. Y. Parkhomenko, Phys. Lett. B **595**, 323 (2004).
[6] B. Aubert *et al.* (*BABAR* Collaboration), Phys. Rev. Lett.

98, 151802 (2007).
[7] L. Breiman, Mach. Learn. **24**, No. 2, 123 (1996).
[8] B. Aubert *et al.* (*BABAR* Collaboration), Nucl. Instrum. Methods Phys. Res., Sect. A **479**, 1 (2002).
[9] S. Agostinelli *et al.* (GEANT4 Collaboration), Nucl. Instrum. Methods Phys. Res., Sect. A **506**, 250 (2003).
[10] G. C. Fox and S. Wolfram, Nucl. Phys. **B149**, 413 (1979).
[11] B. Aubert *et al.* (*BABAR* Collaboration), Phys. Rev. Lett. **89**, 201802 (2002).
[12] C. Amsler *et al.* (Particle Data Group), Phys. Lett. B **667**, 1 (2008).
[13] J. E. Gaiser *et al.* (Crystal Ball Collaboration), Phys. Rev. D **34**, 711 (1986).
[14] H. Albrecht *et al.* (ARGUS Collaboration), Z. Phys. C **48**, 543 (1990).
[15] C.-D. Lu *et al.*, Phys. Rev. D **72**, 094005 (2005).
[16] C. Kim, A. K. Leibovich, and T. Mehen, Phys. Rev. D **78**, 054024 (2008).
[17] S. W. Bosch and G. Buchalla, J. High Energy Phys. 01 (2005) 035.
[18] D. Mohapatra *et al.* (Belle Collaboration), Phys. Rev. Lett. **96**, 221601 (2006); N. Taniguchi *et al.* (Belle Collaboration), Phys. Rev. Lett. **101**, 111801 (2008); **101**, 129904(E) (2008).